Microfluidic Technique for the Simultaneous Quantification of Emulsion Instabilities and Lipid Digestion Kinetics

Nathalie Scheuble, Alexander Iles, Robert C. R. Wootton, Erich J. Windhab, Peter Fischer and Katherine S. Elvira

2017

https://dx.doi.org/10.1021/acs.analchem.7b01853

A microfluidic technique for the simultaneous quantification of emulsion instabilities and lipid digestion kinetics

Nathalie Scheuble,[†] Alexander Iles,[‡] Robert C. R. Wootton,[¶] Erich J. Windhab,[†] Peter Fischer,[*,†] and Katherine S. Elvira[*,§]

Institute of Food Nutrition and Health, ETH Zurich, 8092 Zurich, Switzerland, School of Mathematics and Physical Sciences, Department of Chemistry, Hull, HU6 7RX, UK, Department of Science and Technology, Ipswich, IP4 1QJ, UK, and Department of Chemistry, Victoria BC, V8W 2Y2, Canada

E-mail: peter.fischer@hest.ethz.ch; kelvira@uvic.ca

Abstract

Quantifying the impact of environmental physicochemical changes on the micro-structure of lipid delivery systems is challenging. We have therefore developed a methodology to quantify the coalescence of oil-in-water emulsion droplets during lipid digestion *in situ* on a single droplet level. This technique involves a custom-made glass microfluidic platform, in which oil droplets can be trapped as single droplets, or several droplets per trap, the physicochemical environment can be controlled, and droplet digestion, as well as coalescence, can be visualized.

[*]To whom correspondence should be addressed
[†]ETH Zurich
[‡]University of Hull
[¶]University of Suffolk
[§]University of Victoria

We show that the exchange of the physicochemical conditions in the entire reaction chamber can be reached in under 30 s. Microparticle image velocimetry allowed mapping of the flow profile and demonstrated the tuneability of the shear profile in the device. The extraction of quantitative information regarding the physical characteristics of droplets during digestion was performed using automated image analysis throughout the digestion process. Therefore, we were able to show that oil-in-water emulsions stabilized by proteins coalesced under human gastric conditions. This coalescence delayed the overall lipid digestion kinetics. Droplets that coalesced during digestion were hydrolized 1.4 times slower than individually trapped droplets. Thus, the micro-structural evolution of lipid delivery systems is a crucial factor in lipid digestion kinetics. This novel technique allows the simultaneous quantification of the impact that the physicochemical environment has on both lipid droplet micro-structure and on lipid release patterns.

Keywords: lipid digestion, lipid-based delivery systems, microfluidics, emulsion instabilities, kinetics, coalescence, droplet micro-structure.

Introduction

The study of fat digestion mechanisms is important to understand the release of poorly water-soluble drugs and functional food ingredients that are dispersed in lipids. During human digestion, emulsified lipids undergo various physicochemical changes that affect their microstructure, as has been discussed by various authors for bulk emulsion systems.[1–5] For example, they may flocculate or coalesce. Concurrently, lipolytic enzymes (lipases) adsorb to oil/water interfaces and hydrol-yse lipids to aid lipid absorption into the body. This digestion of lipid emulsion droplets, which causes an overall decrease in droplet size, and the transformation of emulsion microstructure dur-ing digestion, which can cause an increase in droplet size, occur simultaneously and influence each other.[6,7] Data obtained from conventional analytical techniques such as the pH-stat technique or gas chromatography[8] are therefore a superposition of those mechanisms. Thus, quantifying emulsion microstructure during digestion is challenging and has only recently been addressed using

confocal microscopy on the level of individual droplets.[9] However, controlling the surrounding aqueous phase was not performed in these studies. Here we have developed a methodology to quantify coalescence of emulsion droplets during digestion *in situ* on a single droplet level using a glass microfluidic platform. Lipid oil droplets formed using medium-chain triglycerides (MCT) as a model system were initially created in an aqueous buffer containing a stabilising agent, β -lactoglobulin (β -lg) as a model for a protein based emulsifier commonly used by the food or pharmaceutical industry. After droplet generation, the aqueous phase was exchanged for an aqueous phase that represents a simplified composition of the human gastrointestinal environment. The influence of pepsin was not studied because gastric lipase is particularly prone to proteolysis at the low pH values where pepsin is usually active. Bile salts were omitted for the sake of fluid stability.

This microfluidic platform allows the visualization and analysis of emulsion structure while controlling the physicochemical conditions of the environment. Microfluidic technologies are designed to allow fluid manipulation on the micrometer scale and have been developed for a variety of different applications such as chemical synthesis,[10] single cell analysis[11] and artificial membranes.[12] An important subsection of the field are droplet microfluidic devices, where pico- to nanoliter volume droplets of one fluid (normally aqueous) can be created in another continuous fluid (normally oil).[13] Microfluidic platforms have previously been used to study the coalescence of emulsion droplets,[14–17] the stability of double emulsions[18], and the lipid digestion of single droplets,[19] but a platform, such as the one proposed here, for the study of lipid digestion (lipolysis) and coalescence under different gastric conditions, is completely novel.

Experimental section

Two separate microfluidic devices were used in each experiment: One solely to produce the emulsion droplets and another to trap the droplets and study the influence of physicochemical properties on emulsion structure and digestion. An overview on the experimental setup is given in Figure S1.

Microfluidic droplet trapping device fabrication

Schott B270 glass blank wafers (3 mm thick) and wafers pre-coated with low reflective chromium and photoresist (1.15 mm thick) were obtained from Telic (California, USA). The coated wafers were micro-patterned with traps designed in AutoCAD (Autodesk, USA) using UV photolithography. The glass was wet-etched to the desired depth (37 μm) using buffered $HN0_3$/HF solution. After etching, access holes were drilled in the 3 mm blank layers using a CNC machine (Datron, Milton Keynes, UK). The wafer surfaces were then degreased with acetone followed by isopropanol, and immersed in heated piranha solution for one hour. Clean wafers were subsequently washed with deionized water. The structured wafers were then aligned with the blank wafers containing the access holes and thermally bonded together by applying slight pressure and heating to 585°C for 10 hours in air. After bonding, chopped off Luer tips of polypropylene syringes were glued into the access holes using Al-Fix Gel (Novatio, Switzerland) to provide an access interface. The layout of the microfluidic droplet trapping device, a microscopy image of the array of droplet traps, and the theoretical shape of a trap before and after etching are shown in Figure 1.

Droplet formation and trapping

Droplets were created using a T-junction geometry on a glass microfluidic device purchased from Micronit (FC_TSDG.C, The Netherlands). To produce droplets with sizes between 35 and 40 μm in diameter, the flow rate of the dispersed phase was 0.2 μL/min and that of the continuous phase was between 34 and 37 μL/min. The final volume fraction of the dispersed oil droplet was approximately 0.6 vt%. The emulsion was feet into the microfluidic trapping platform so that either individual or several droplets were captured by the traps. Droplets remaining between the traps were flashed away after filling the microfluidic trapping platform. The dispersed phase consisted of MCT oil (BASF, Germany) with 12.5 μg/mL Nile red (Sigma Aldrich, Germany) and the continuous phase consisted of 2.5% β-lactoglobulin (β-lg) and 10 mM PBS - phosphate buffer solution at pH 7. Flow rates were controlled using two syringe pumps (Harvard Pump Apparatus, USA) with 0.5 or 1 mL glass gastight syringes (Hamilton, Switzerland). The continuous and

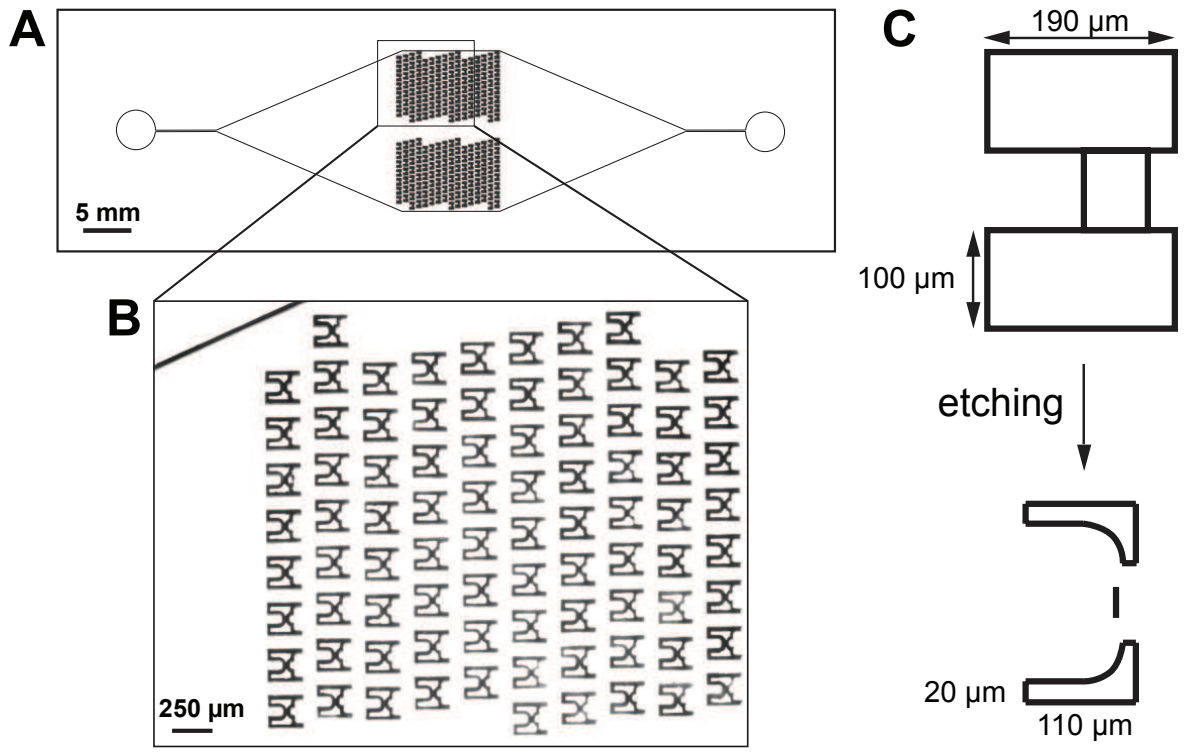

Figure 1: Design of the microfluidic droplet trapping device. The glass microfluidic device contained 2 sections, each with 14 rows of between 8 and 9 traps each (238 traps in total). The device was isotropically etched to a depth of 37 μm. (A) Scale drawing of the device, showing the two sections of traps (top and bottom) within the large diamond-shaped reaction chamber. The access holes to the device have a diameter of 4.1 mm and the device has an overall footprint of 17x38 mm. (B) Light microscopy image of a section of the microfluidic device showing the etched traps. (C) Scale drawings of the trap design before and after etching. The line shown between the upper and lower section of the etched trap denotes a weir with a targeted height of approximately 24 μm.

dispersed phases were filtered prior to use using a 0.45 μm cellulose acetate filter and a 0.2 μm PTFE filter (VWR International, Switzerland), respectively. The emulsion was collected in a vial and stored at 4°C overnight to allow complete establishment of the interfacial protein layer built by β-lg.[20]

Droplets were then inserted into the glass microfluidic droplet trapping device. The entire set-up is provided in Figure S1. At the start of each experiment, the microfluidic device was flushed with MilliQ water, then with a 1 % solution of Caraform Universal (Dr. Weigert GmbH & Co, Switzerland) to throughly clean the device and allow uniform wetting and easy removal of air bubbles. Subsequently, the microfluidic device was flushed with at least 5 ml of MilliQ water, put inside a custom-made stainless steel chamber to allow optimal heat transfer, placed on a heating stage (PE 94, Linkam, Japan) and connected via tubing (polytetrafluoroethylene, PTFE, inner diameter = 250 μm, 1/16 inch outer diameter Polyflon Technology Limited, UK) to a valve (V-100L, Ercatech, Switzerland). This valve was used to seamlessly switch the fluid injected into the device without disconnecting the syringes. A glass syringe was filled with the protein stabilized droplets created in the Micronit device and the microfluidic droplet trapping device was gently filled with the emulsion. Once the traps were full, droplets outside of the traps and the bulk aqueous phase were removed by flushing the microfluidic device with 200 μL of MilliQ water at a flow rate of 50 μL/min. Figure 2 shows a light microscopy image and a fluorescence image of a microfluidic device filled with droplets in such a way.

Droplet digestion

After filling the microfluidic trapping device with droplets, the heating stage was set to 38.5°C to reach 37°C inside the chamber. This was measured inside the chamber using a type K thermo-couple (Thermocontrol GmbH, Switzerland). Digestive fluids, designed to mimic either gastric or pancreatic lipolysis were then injected into the device. The flow rate was initially set at 50 μL/min for 100 s to ensure exchange of the entire bulk phase and then at 1 μL/min for the duration of the experiment. Fluids mimicking gastric lipolysis consisted of 50 mM citric acid buffer at pH 5

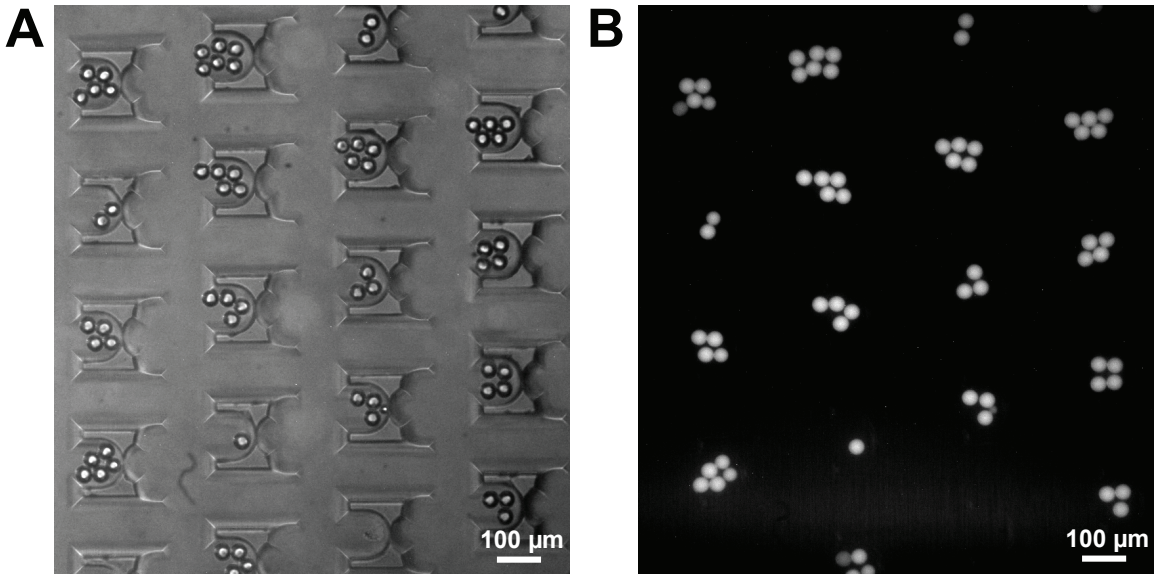

Figure 2: Microfluidic traps filled with MCT oil droplets. (A) Light microscopy image and (B) laser induced fluorescent image of the microfluidic device filled with MCT oil droplets dosed Nile red and stabilized by β-lg.

and 0.5 mg/mL recombinant dog gastric lipase (rDGL). rDGL had an activity of 183 $\pm$ 24 U/mg when using a standard gastric lipase assay. Fluids mimicking pancreatic lipolysis consisted of 70 mM PBS buffer at pH 7 and 17 mg/mL porcine pancreatic lipase (PL, pancreatin, Sigma-Aldrich, Switzerland) to reach an activity of 2000 U/mL. Pancreatic lipase activity was measured using the pH-stat technique under the conditions proposed in Minekus *et al.* (2014).[21] PL was dissolved in the buffer by vortexing for 15 s and was then centrifuged at 13.5 g for 5 min to remove solid particles. High buffer strengths were chosen to ensure that pH was constant throughout the experiment, since lipase activity is pH-dependant, and an ionic strength of 150 mM is required to reproduce physiological conditions. Flow rates during lipolysis were set to 1 μL/min to create gentle experimental conditions for digestion and reduce the effect of interfacial shear forces. At higher flow rates (5 - 10 mL/min) droplets escaped the traps.

Imaging and image analysis

An inverted microscope (Leica DM-IRB, Switzerland) with an 10x objective (NA0.3, air immersion, Leica, Switzerland) was used to acquire light microscopy images of MCT oil droplets stained with Nile red, fluorescent particles (1 μm, Fluoromax, Switzerland), and of the aqueous phase stained with Rhodamine 6G (Fluka, Switzerland). To generate fluorescent images, a Nd:YAG laser supplying monochrome light with a wavelength of 1.064 nm was used. This laser beam was passed through polarization filters generating a wavelength of 532 nm pulsed at the desired frequency. These pulses passed through an epifluorescent prism assembly (Y3 filter, Leica, Switzerland) before the fluorescent signal was transferred to the camera. The double pulsed laser was only used for microparticle image velocimetry (μPIV) experiments, which were used to map and visualize the flow within the microfluidic droplet trapping device. The solution of fluorescent particles was extensively diluted (100-1000 times depending on flow rate and maginfication) in MilliQ water to imitate the fluid dynamics of a dilute aqueous system. The local vectors of particle dislocations were determined by cross-correlating frames originating from double-pulsed laser images using image processing software (DynamicStudio, version 3.41). Rhodamine 6G was used to visualize the phase exchange in the microfluidic device.

MCT oil droplets were stained with Nile red to be able to perform image analysis during the digestion experiments. The images taken of these fluorescent droplets were then processed using automated image analysis software (Cellprofiler, version 2.1.1) to measure droplet diameter. Figure 3 shows an example of the processed image data superimposed on the original images using Cellprofiler.

Droplet volume V, and surface area A, of droplets with diameter d larger than 37 μm, and thus of a size larger than the height h_c of the microfluidic device were calculated separately using the formula developed by Binks[22] for round disk-like particles:

$$V = \frac{4}{3}\pi h_c^3 \left[\frac{3(d/h_c - 1)^2}{2} + \frac{3\pi(d/h_c - 1)}{4} + 1 \right] \quad (1)$$

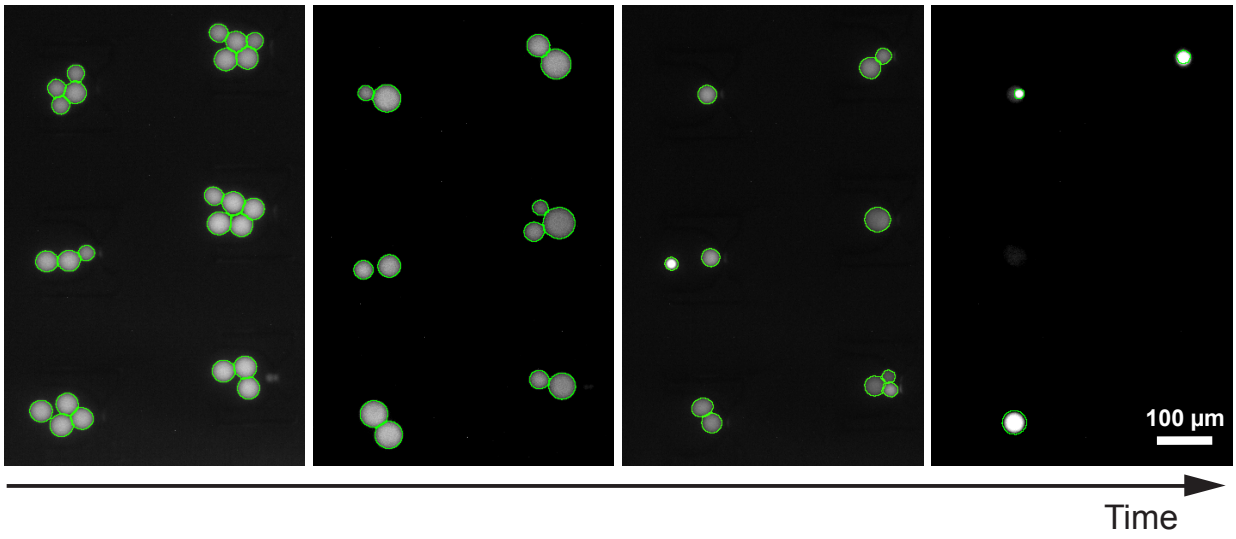

Figure 3: Images of fluorescent MCT oil droplets trapped in the microfluidic device during lipid digestion, showing how coalescence and digestion occur over time. The images are superimposed with the result (outlined in green) of automated image analysis using Cellprofiler.

$$A = 2\pi h_c^2 \left[\left(\frac{d}{h_c} - 1 \right)^2 + \pi \left(\frac{d}{h_c} - 1 \right) + 2 \right] \tag{2}$$

The solubilized volume of MCT oil, V_{sol}, over time was then calculated from the apparent total volume of all droplets, $V_{tot,app}$ (measured using Cellprofiler from experimental images), and the initial total volume of all droplets, $V_{tot,in}$ as follows:

$$V_{sol} = \left(1 - \frac{V_{tot,app}}{V_{tot,in}} \right) \times 100 \tag{3}$$

V_{sol} represents the amount MCT oil, which solubilized during lipid digestion and is a measure of lipid digestion kinetics.

Results and discussion

Device characterization

The internal flow field of the microfluidic device was mapped using μPIV. Figure 4A shows local vectors of the flow profile at various flow rates. Two major flow regions were identified. High shear flow regions occur between the rows of traps (in the direction of flow), and low shear flow regions occur inside the traps and between the columns of traps (perpendicular to the direction of flow). The shear rates were proportional to the flow rate and thus could be adapted to create the desired shear profile. When the device was filled with droplets, particles still flowed inside the traps and between the droplets (Figure 4B).

However, more dead zones appeared, in which the displacement of the particles and thus the shear rates were lower. These observations are approximate since the particle size (1 μm) is much larger than the lipase molecules that cause droplet digestion. We can assume that lipase molecules will be more evenly distributed throughout the device and should therefore be able to access all droplets for digestion. To confirm this assumption regarding the distribution of lipase molecules, the time required to exchange the entirety of the aqueous phase within the microfluidic device was investigated using Rhodamine 6G fluorescent dye. The aqueous solution was injected at a constant flow rate of 50 μL/min and the fluorescent signal was recorded as a function of time (Figure S2). Figure S2 shows the fluorescent dye appearing within the microfluidic device in under 10 s, the intensity of the dye increased for another 10 s, and no change in intensity was detected between 20 and 30 s. Thus, the entire solution in the device was fully exchanged after less than 30 s, that is after 30 μL of fluid had been inserted into the device. To ensure complete phase exchange during the experiments, the device was first flushed with 80 μL of the desired lipase solution at a flow rate of 50 μL/min before the flow rate was adjusted to 1 μL/min for the rest of the experiment.

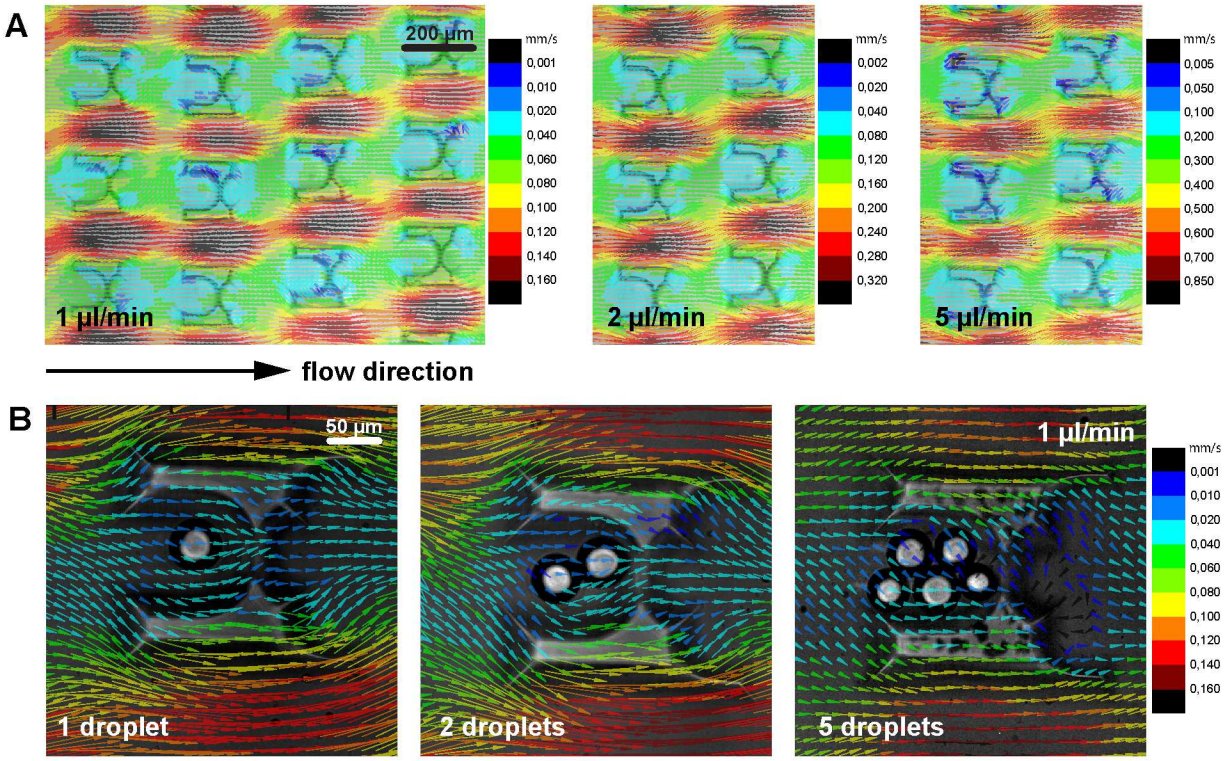

Figure 4: Vector graphics of the internal flow field of the microfluidic device superimposed with light microscopic images of (A) an empty device flushed with an aqueous solution of fluorescent microparticles in MilliQ water at flow rates of 1, 2, and 5 μL/min respectively (the first image shows the uniform distribution of the flow field over a larger section of the microfluidic device). (B) traps filled with 1, 2, or 5 droplets flushed with an aqueous solution at a flow rate of 1 μL/min. In both A and B the scale bars apply to all images and the color code shows the flow velocity in mm/s.

Interdependence of emulsion microstructure and lipid digestion

Here we show representative examples of how emulsion microstructure and lipid digestion can be investigated simultaneously. Microscopy images of trapped fluorescent MCT oil droplets were taken during gastric digestion (0.5 mg/mL rDGL, 50 mM citric buffer, pH 5) followed by pancreatic lipolysis (17 mg/mL pancreatic lipase, 70 mM PBS, pH 7). Figure 5 shows images of traps in the microfluidic device containing several (number of droplets, $n_d = 5$) and single ($n_d = 1$) droplets stabilized by β-lg during lipolysis.

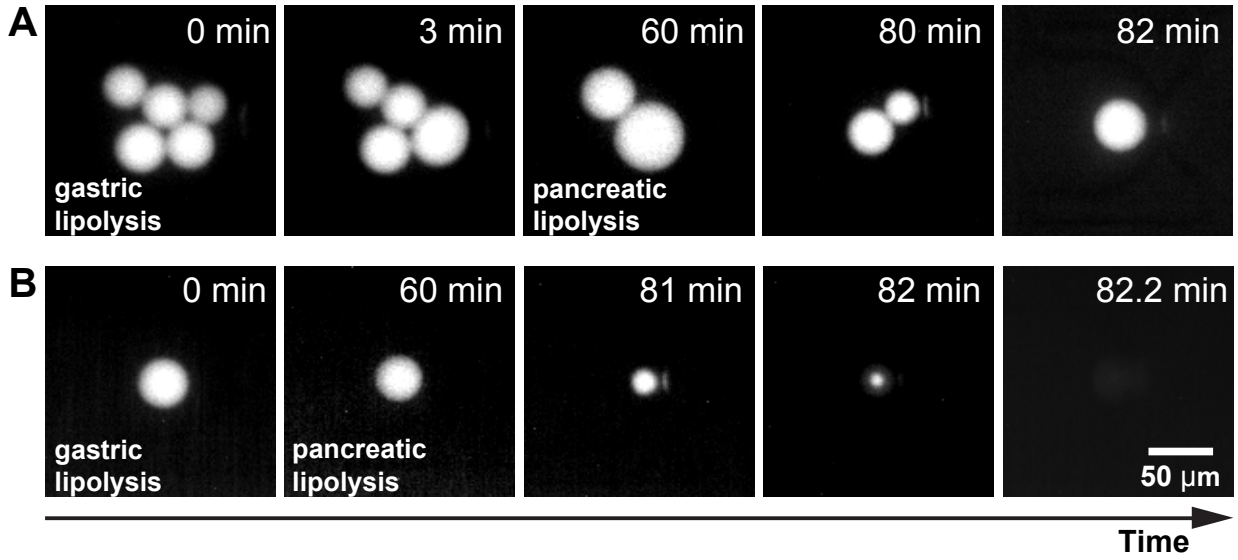

Figure 5: Representative images of MCT oil droplets stabilized by β-lg during gastric lipolysis (0 to 60 min; 0.5 mg/mL rDGL, 50 mM citric buffer, pH 5) followed by pancreatic lipolysis (60 min to end; 17 mg/mL pancreatic lipase, 70 mM PBS, pH 7) over time for (A) several ($n_d = 5$) droplets and (B) a single ($n_d = 1$) droplet per trap. The scale bar applies to all images.

Traps containing several ($n_d = 5$) droplets showed partial coalescence of the droplets during the gastric and pancreatic phases before the MCT oil was fully digested. Experiments with a single ($n_d = 1$) droplet per trap, which could not undergo coalescence, showed that single droplets were digested faster. The decrease in MCT oil droplet size during lipolysis can be attributed to the partial solubilization of lipolytic products from the MCT oil during lipolysis. Therefore, a reduction in droplet size is visible even in the absence of bile salts, which are known to micellize lipolytic products.[23]

Image analysis was performed to extract quantitative information from the droplet images acquired during digestion to investigate the impact of emulsion microstructure on lipolysis kinetics. Figures 6A and 6B show representative data for the mean droplet diameter and the solubilized MCT oil volume of droplets trapped individually or with several droplets per trap as a function of digestion time when using rDGL for gastric lipolysis. Gastric lipolysis is often omitted in *in vitro* digestion experiments since gastric lipases are not commercially available and therefore their relevance is often underestimated.

Whereas the mean droplet diameter increased during coalescence, it decreased with MCT oil hydrolysis (lipolysis). Therefore, the size of single trapped droplets decreased linearly during the gastric phase and faster during the pancreatic phase. An acceleration of this diameter decrease was observed within the last 50 - 100 s before the complete solubilization of all lipolytic products occurred (Figure 6A). These kinetics correlated to the solubilized MCT oil volume, which is shown as a function of time in Figure 6B. Within one hour, 22 % of the total MCT oil volume was solubilized by rDGL, and the remaining MCT oil volume was solubilized almost 10 times faster during pancreatic lipolysis. These data for digestion time and lipid release patterns are similar to those typically found *in vivo*.[24]

For $n_d = 5$ trapped droplets, two primary coalescence periods were identified, one at the start of the gastric lipolysis phase and the other towards the end of the pancreatic lipolysis phase. Therefore, mean droplet sizes increased during these periods. Whereas during the initial gastric phase coalescence occurred due to changing environmental conditions, coalescence during the pancreatic phase may have been induced due to the accumulation of high amounts of lipolytic products inside the MCT oil droplets. Fatty acids might be directly solubilized during lipolysis, whereas diglycerides might accumulate inside the droplet and at the oil/water interface since they are themselves surface active.[25,26] These diglycerides may dominate interfacial dynamics and cause concentration gradients and inhomogeneity within the interfacial layer (Marangoni effects[27]), which can lead to emulsion instabilities. Control experiments (see Figure S3) show that the lack of pancreatic lipase does not affect either the droplet size or the digested oil volume.

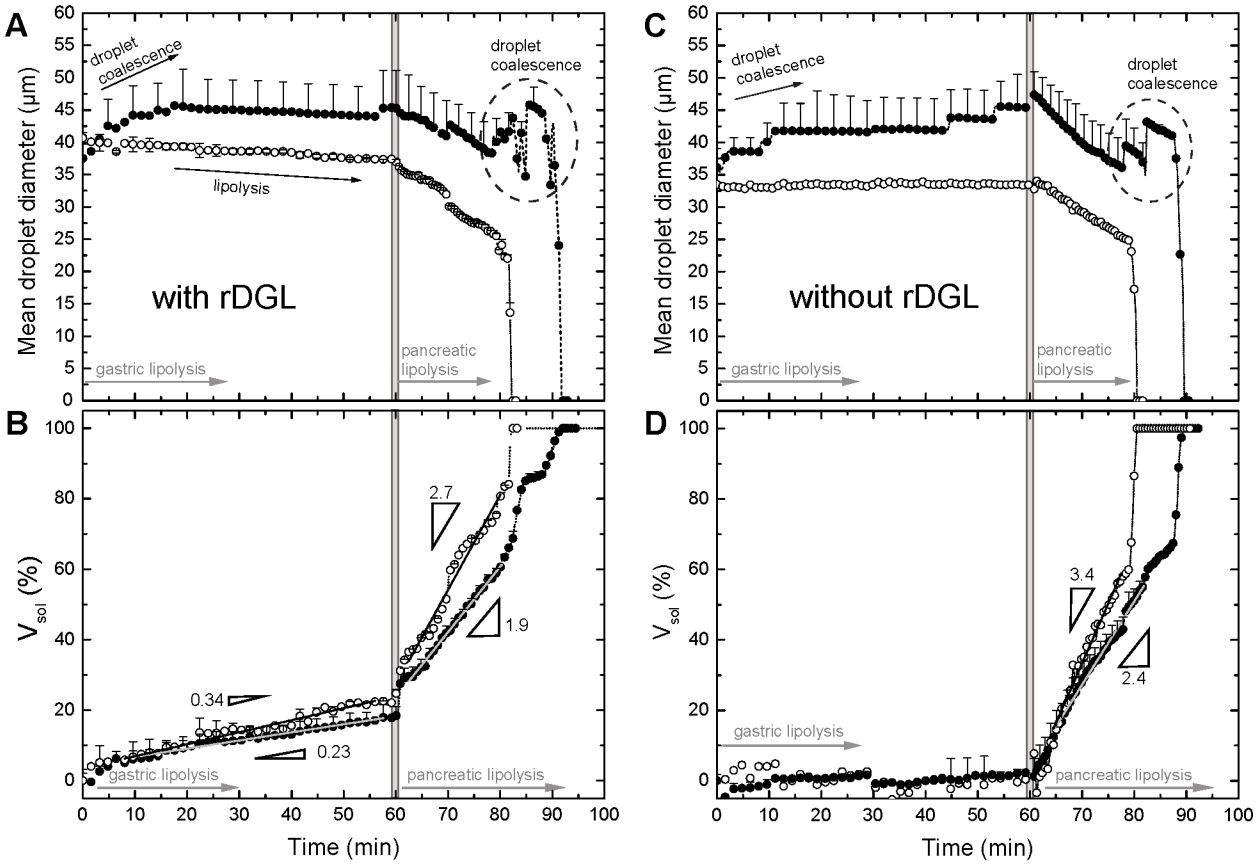

Figure 6: (A) Change in the mean droplet diameter and (B) cumulative digested MCT oil volume, V_{sol}, of $n_d = 1$ and $n_d = 5$ trapped droplets during gastric lipolysis (0 to 60 min) using rDGL and pancreatic lipolysis (60 min to end) using pancreatin. Data show that single droplets have an approximately 1.4 times higher solubilization rate than when $n_d = 5$ droplets are contained in a trap. The triangles indicate the slope of the linear fit. In both A and B white circles represent data acquired over time for the digestion of a single trapped droplet and black circles represent data acquired over time for the digestion of $n_d = 5$ trapped droplets. (C) Change in the mean droplet diameter and (D) cumulative digested MCT oil volume, V_{sol}, of $n_d = 1$ and $n_d = 5$ trapped droplets during gastric lipolysis (0 to 60 min) without rDGL, and pancreatic lipolysis (60 min to end) using pancreatin. Data show that single droplets have an approximately 1.4 times higher solubilization rate than when $n_d = 5$ droplets are contained in a trap. Triangles indicate the slope of the linear fit. In both A and B white circles represent data acquired over time for the digestion of a single trapped droplet and black circles represent data acquired over time for the digestion of $n_d = 5$ trapped droplets. Control experiments without pancreatic lipase or rDGL are shown in the Supporting Information. The data represent results from independent droplet digestion processes in multiple traps.

Furthermore, β-lg might be digested by proteolytic enzymes present in the pancreatin used and therefore droplets might be further destabilized.[28] Additionally, Laplace pressure increases with decreasing droplet size. Therefore, small droplets either solubilize or coalesce into bigger droplets. After coalescence during pancreatic lipolysis, droplets were solubilized rapidly within 200 s. In between these coalescence periods droplet sizes decreased constantly during gastric lipolysis and faster during pancreatic lipolysis. However, emulsion microstructure influenced the lipolysis rate significantly, since it correlates with the specific surface area of the droplet. The influence of microstructure on the solubilization of MCT oil is shown in Figure 6. During both gastric and pancreatic lipolysis, the MCT oil solubilization rate was about 1.4 times larger for single (n_d = 1) droplets compared to n_d = 5 trapped droplets.

To distinguish between the role of rDGL and the role of the physicochemical conditions present in the gastric environment on emulsion microstructure, the same experiment described above was performed without rDGL. Figures 6C and 6D show the evolution of droplet size and volume of solubilized MCT oil for single and n_d = 5 droplets as a function of time. No change in volume content occurred under gastric conditions (pH 5, 50 mM citric acid buffer). However, coalescence occurred during the entire gastric phase. pH 5 is the optimum pH for human gastric lipolysis,[29] but it is also the isoelectric point of β-lg. This causes a decrease in electrostatic repulsion between β-lg covered droplets and therefore they are likely to coalesce. Moreover, the interfacial film formed by β-lg increases in viscoelasticity at pH 5,[30,31] which indicates that β-lg agglomerates on the droplet interface and thus defects in the membrane covering the droplet are more likely to occur.

In contrast to experiments performed with rDGL, during control experiments without rDGL coalescence was observed during the entire gastric phase. Thus, lipolytic products produced from rDGL might stabilize a gastric emulsion. However, changing the on-chip conditions to those that mimic pancreatic lipolysis shows clearly the impact of emulsion microstructure on the lipid solubilization rate during pancreatic lipolysis, since, again single droplets were solubilized around 1.4 times faster than coalesced droplets. Comparing these results to Figures 6A and 6B shows that even without rDGL the droplets were solubilized slightly earlier (t = 91.8 min for experiments with

rDGL and t = 89.6 min for experiments without rDGL). This effect can be attributed to a lower initial droplet size and therefore higher specific interfacial area.[32] Thus the specific interfacial area has a greater effect on the total MCT oil solubilization time than gastric lipolysis.

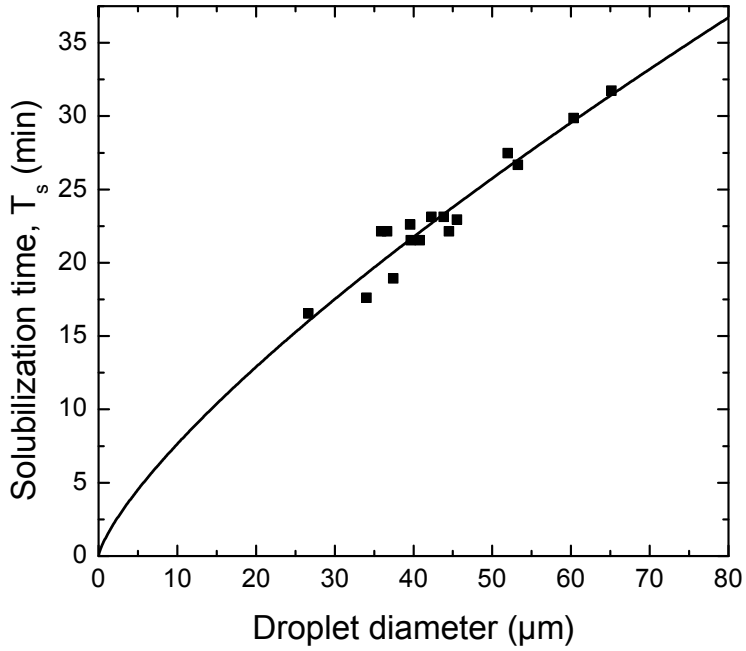

Figure 7: Complete MCT oil solubilization time, T_s, as a function of droplet diameter, d. Data were empirically fitted using a power law equation. Data shown in this figure were collected from three individual experiments, demonstrating the robustness of the technique.

Therefore, the impact of the droplet diameter, d, of single trapped droplets, which directly correlates with the specific interfacial droplet area, on the complete solubilization time, T_s, caused by pancreatic lipolysis was assessed. As shown in Figure 7, the specific interfacial area available for lipolysis and thus the droplet diameter, greatly influenced the MCT oil solubilization time. Data were fitted using the following power law equation for the solubilization time $T_s = 1.34 \cdot d^{0.755}$. This shows not only that smaller droplets are digested much faster, but that the importance of droplet size increases with decreasing droplet size. Extrapolation of this fit emphasizes that micron-sized droplets are solubilized within minutes, which is within the same time frame as seen for the solubilisation of unstructured, diluted emulsions measured in bulk. Thus, analyzing single droplets using microfluidic technologies might represent a diluted emulsion system, in which the bulk phase and droplet density are of minor importance. However, coalesced droplets always lead

to decreased specific interfacial area and therefore have a major impact on lipolysis.

Conclusions

The microfluidic platform developed herein allows the quantification of emulsion microstructure and lipid digestion simultaneously. Furthermore, the physicochemical environment can be controlled and exchanged within less than 30 s. This not only guarantees an efficient exchange of the bulk phase, but continuous renewal of digestive juices and removal of digested products throughout the experiment. Therefore we are able to analyse specific droplets under different conditions over time, allowing the acquisition of size-dependant digestion information, as well as bulk data.

Emulsion coalescence mainly occurred during the gastric phase. This had a major influence on pancreatic lipolysis, since the related droplet diameter increase correlates with the specific area of the droplet. Individually (n_d = 1) trapped droplets were therefore digested 1.4 times faster than n_d = 5 trapped droplets. Droplet size was the main contributor to total MCT oil solubilization during pancreatic lipolysis. Even though gastric lipolysis contributed to around 20% of the overall digestion, it had a minor effect on MCT oil solubilization time during pancreatic lipolysis since the solubilization rate during pancreatic lipolysis was almost 10 times faster. Thus, the microstructure generated in human gastric environments contributes crucially to lipid digestion and should not be omitted in *in vitro* experiments to improve *in vitro-in vivo* correlations.

To conclude, emulsion microstructure determines lipolysis kinetics and is therefore a crucial parameter when designing lipid delivery systems. The potential of this method not only lies in the quantification of instabilities of lipid delivery systems, but in the *in situ* visualization of lipase adsorption, displacement processes, and lipid release by combining the technique, for example, with confocal microscopy. Our future experiments focus on the influence of different physicochemical conditions (lipid phase, emulsifier type) on emulsion microstructure during *in vitro* lipolysis.

Acknowledgement

The authors thank Frederic Carrière for providing rDGL, José Toro-Sierra for providing β-lactoglobulin and Manuel Schuhmacher for generating preliminary results. The Swiss National Foundation (SNF) is acknowledged for funding projects No. 2000-21137941 and No. 200020-159898.

S-1

Supporting Information

A Microfluidic Technique for the Simultaneous Quantification of Emulsion Instabilities and Lipid Digestion Kinetics

Nathalie Scheuble[1], Alexander Iles[2], Robert C. R. Wootton[3], Erich J. Windhab[1], Peter Fischer[*,1], Katherine S. Elvira[*,4]

[1]*Institute of Food Nutrition and Health, ETH Zurich, 8092 Zurich, Switzerland*
[2]*School of Mathematics and Physical Sciences, Departement of Chemistry, Hull, HU6 7RX, UK*
[3]*Department of Science and Technology, Ipswich, IP4 1QJ, UK*
[4]*Department of Chemistry, Victoria BC, V8W 2Y2, Canada*

This supporting information contains a picture of the entire experimental set-up to provide a clearer idea of the experiment. Furthermore, it contains a measurement confirming the fluid phase exchange within the microfluidic platform. Finally, a reference measurement shows that without lipases addition the droplets do not solubilize.

Table of Content

S-2

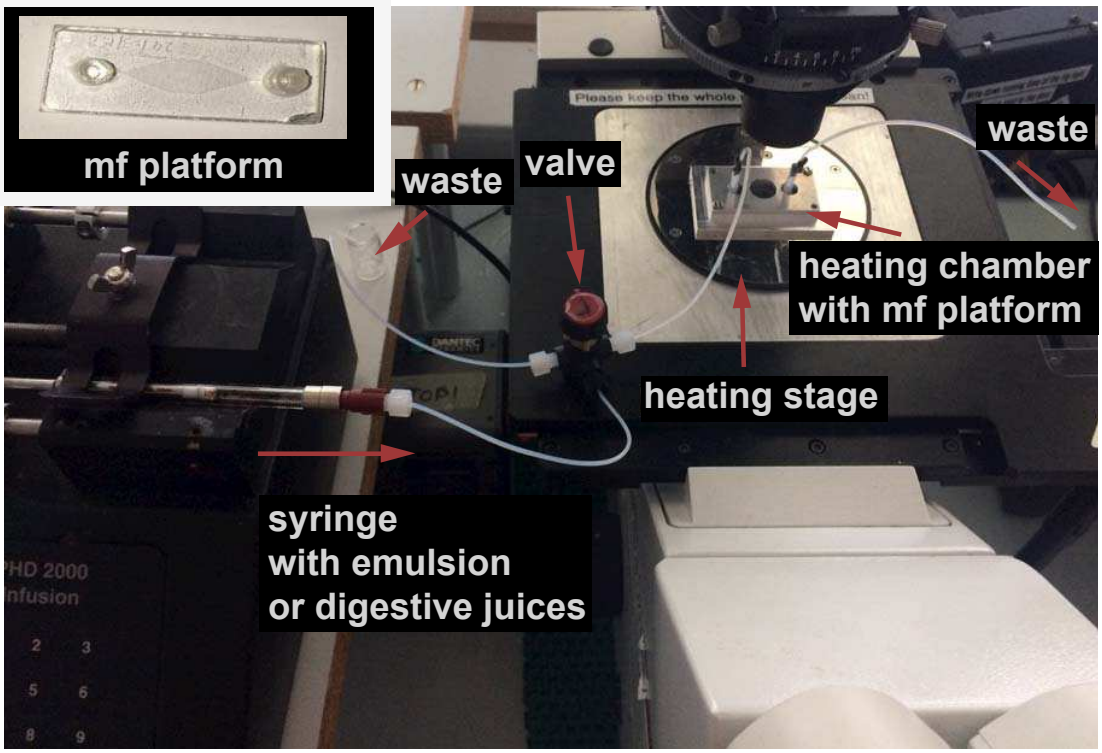

Figure S1: Picture including the description of the experimental set up.

S-3

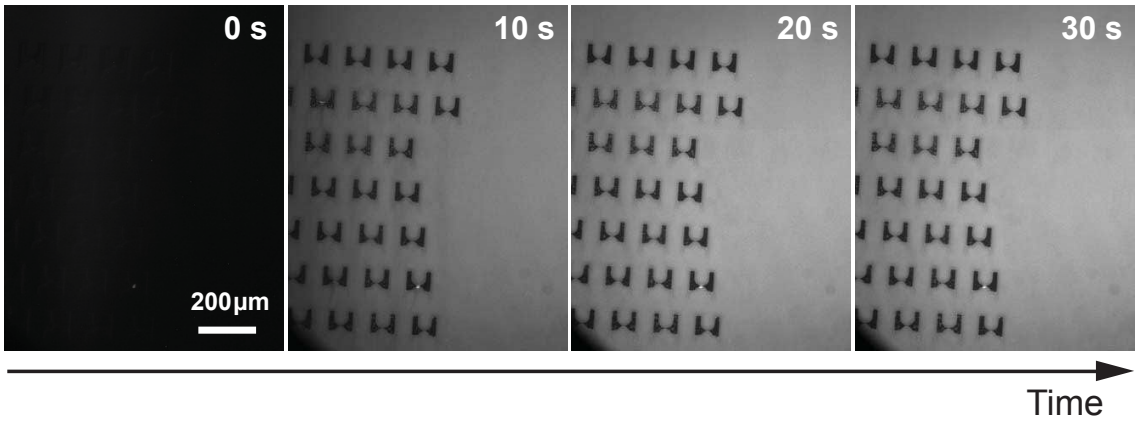

Figure S2: Microscopy images of the microfluidic device over time while an aqueous solution containing Rhodamine 6G was flushed through the device at a flow rate of 50 µl/min. After less than 30 s the entire phase was exchanged.

S-4

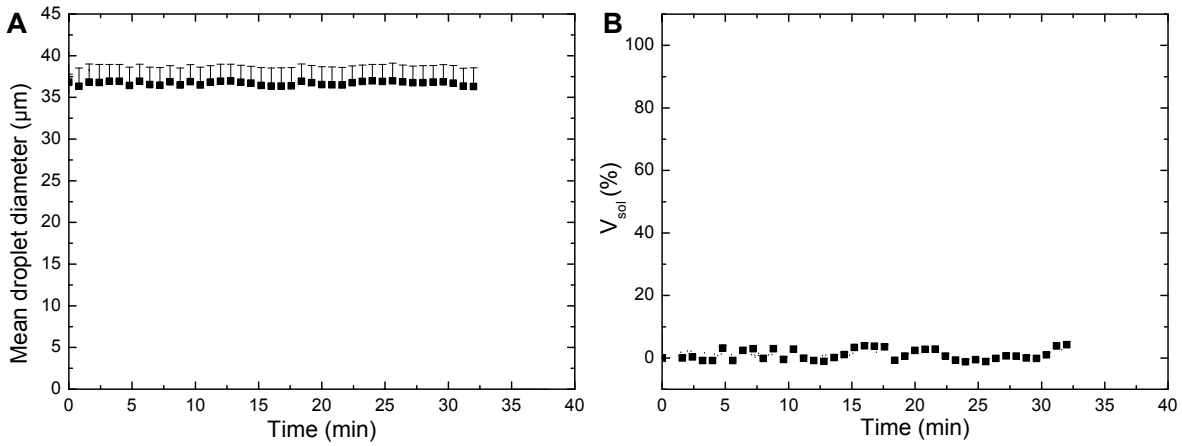

Figure S3: (A) Change in the mean droplet diameter and (B) cumulative digested MCT oil volume, V_{sol}, for several trapped droplets (all droplets in image) as a function of time while flushing with 70 mM PBS at pH7 without pancreatic lipase.

References

[1] Golding, M.; Wooster, T. J. The influence of emulsion structure and stability on lipid digestion. *Curr. Opin. Colloid Interface Sci.* **2010**, *15*, 90–101.

[2] Golding, M.; Wooster, T. J.; Day, L.; Xu, M.; Lundin, L.; Keogh, J.; Clifton, P. Impact of gastric structuring on the lipolysis of emulsified lipids. *Soft Matter* **2011**, *7*, 3513–3523.

[3] Seimon, R. V.; Wooster, T.; Otto, B.; Golding, M.; Day, L.; Little, T. J.; Horowitz, M.; Clifton, P. M.; Feinle-Bisset, C. The droplet size of intraduodenal fat emulsions influences antropyloroduodenal motility, hormone release, and appetite in healthy males. *Am. J. Clin. Nutr.* **2009**, *89*, 1729–1236.

[4] Lundin, L.; Golding, M.; Wooster, T. J. Understanding food structure and function in developing food for appetite control. *Nutrition & Dietetics* **2008**, *65*, S79–S85.

[5] Marciani, L.; Faulks, R.; Wickham, M. S. J.; Bush, D.; Pick, B.; Wright, J.; Cox, E. F.; Fillery-Travis, A.; Gowland, P. A.; Spiller, R. C. Effect of intragastric acid stability of fat emulsions on gastric emptying, plasma lipid profile and postprandial satiety. *Br. J. Nutr.* **2009**, *101*, 919–928.

[6] Armand, M.; Pasquier, B.; André, M.; Borel, P.; Senft, M.; Peyrot, J.; Salducci, J.; Portugal, H.; Jaussan, V.; Lairon, D. Digestion and absorption of 2 fat emulsions with different droplet sizes in the human digestive tract. *Am. J. Clin. Nutr.* **1999**, *70*, 1096–1106.

[7] Armand, M.; Borel, P.; Pasquier, B.; Dubois, C.; Senft, M.; André, M.; Peyrot, J.; Salducci, J.; Lairon, D. Physicochemical characteristics of emulsions during fat digestion in human stomach and duodenum. *Am. J. Physiol.: Gastrointest. Liver Physiol.* **1996**, *271*, 172–183.

[8] Beisson, F.; Tiss, A.; Rivière, C.; Verger, R. Methods for lipase detection and assay: a critical review. *Eur. J. Lipid Sci. Technol.* **2000**, *102*, 133–153.

[9] Donato-Capel, L.; Garcia-Rodenas, C.; Pouteau, E.; Kolodziejczyk, E.; Sagalowicz, L. *Food Structures, Digestion and Health*; Academic Press, 2014; pp 389–422.

[10] Elvira, K. S.; Casadevall i Solvas, X.; Wootton, R. C. R.; deMello, A. J. The past, present and potential for microfluidic reactor technology in chemical synthesis. *Nat. Chem.* **2013**, *5*, 905–915.

[11] Rakszewska, A.; Tel, J.; Chokkalingam, V.; Huck, W. T. One drop at a time: toward droplet microfluidics as a versatile tool for single-cell analysis. *NPG Asia Mater.* **2014**, *6*, e133.

[12] Stanley, C. E.; Elvira, K. S.; Niu, X. Z.; Gee, A. D.; Ces, O.; Edel, J. B.; deMello, A. J. A microfluidic approach for high-throughput droplet interface bilayer (DIB) formation. *Chem. Commun.* **2010**, *46*, 1620–1622.

[13] Debon, A. P.; Wootton, R. C. R.; Elvira, K. S. Droplet confinement and leakage: Causes, underlying effects, and amelioration strategies. *Biomicrofluidics* **2015**, *9*, 024119.

[14] Akartuna, I.; Aubrecht, D. M.; Kodger, T. E.; Weitz, D. A. Chemically induced coalescence in droplet-based microfluidics. *Lab Chip* **2015**, *15*, 1140–1144.

[15] Krebs, T.; Schroën, C. G. P. H.; Boom, R. M. Coalescence kinetics of oil-in-water emulsions studied with microfluidics. *Fuel* **2013**, *106*, 327–334.

[16] Krebs, T.; Ershov, D.; Schroen, C. G. P. H.; Boom, R. M. Coalescence and compression in centrifuged emulsions studied with in situ optical microscopy. *Soft Matter* **2013**, *9*, 4026–4035.

[17] Huebner, A. M.; Abell, C.; Huck, W. T. S.; Baroud, C. N.; Hollfelder, F. Monitoring a reaction at submillisecond resolution in picoliter volumes. *Anal. Chem.* **2011**, *83*, 1462–1468.

[18] Jana Bahtz, J.; Gunes, D. Z.; Syrbe, A.; Mosca, N.; Fischer, P.; Windhab, E. J. Quantification of spontaneous W/O emulsification and its impact on the swelling kinetics of multiple W/O/W emulsions. *Langmuir* **2016**, *32*, 5787?5795.

[19] Marze, S.; Algaba, H.; Marquis, M. A microfluidic device to study the digestion of trapped lipid droplets. *Food Funct.* **2014**, *5*, 1481–1488.

[20] Mezzenga, R.; Fischer, P. The self-assembly, aggregation and phase transitions of food protein systems in one, two and three dimensions. *Rep. Prog. Phys.* **2013**, *76*, 046601.

[21] Minekus, M. et al. A standardised static in vitro digestion method suitable for food - an international consensus. *Food Funct.* **2014**, *5*, 1113–1124.

[22] Binks, B. P. *Colloidal particles at liquid interfaces*; Cambridge University Press: Cambridge, 2006.

[23] Hofmann, A. F. The function of bile salts in fat absorption. The solvent properties of dilute micellar solutions of conjugated bile salts. *Biochem. J.* **1963**, *89*, 57–68.

[24] Lengsfeld, H.; Beaumier-Gallon, G.; Chahinian, H.; De Caro, A.; Verger, R.; Laugier, R.; Carrière, F. *Lipases and Phospholipases in Drug Development*; Wiley-VCH Verlag GmbH & Co. KGaA, 2005; pp 195–229.

[25] Reis, P.; Miller, R.; Leser, M.; Watzke, H.; Fainerman, V. B.; Holmberg, K. Adsorption of polar lLipids at the water-oil interface. *Langmuir* **2008**, *24*, 5781–5786.

[26] Reis, P.; Holmberg, K.; Miller, R.; Krägel, J.; Grigoriev, D. O.; Leser, M. E.; Watzke, H. J. Competition between lipases and monoglycerides at interfaces. *Langmuir* **2008**, *24*, 7400–7407.

[27] Langevin, D. In *Annual Review of Fluid Mechanics*; Davis, SH and Moin, P,, Ed.; Annual Review of Fluid Mechanics; Annual Reviews, 2014; Vol. 46; pp 47–65.

[28] Sarkar, A.; Goh, K. K.; Singh, H. Properties of oil-in-water emulsions stabilized *beta*-lactoglobulin in simulated gastric fluid as influenced by ionic strength and presence of mucin. *Food Hydrocolloids* **2010**, *24*, 534–541.

[29] Sams, L.; Paume, J.; Giallo, J.; Carrière, F. Relevant pH and lipase for in vitro models of gastric digestion. *Food Funct.* **2016**, *7*, 30–45.

[30] Scheuble, N.; Lussi, M.; Geue, T.; Carrière, F.; Fischer, P. Blocking Gastric Lipase Adsorption and Displacement Processes with Viscoelastic Biopolymer Adsorption Layers. *Biomacromolecules* **2016**, *17*, 3328–3337.

[31] Scheuble, N.; Geue, T.; Kuster, S.; Adamcik, J.; R, M.; Fischer, P. Mechanically enhanced liquid interfaces at human body temperature using thermosensitive methylated nanocrystalline cellulose. *Langmuir* **2016**, *32*, 1396?1404.

[32] Benzonana, G.; Desnuelle, P. Etude Cinetique de l'Action de la Lipase Pancreatique sur des Triglycerides en Emulsion. Essai d'une Enzymologie en Milieu Heterogene. *Biochim. Biophys. Acta* **1965**, *10*, 121–136.

Graphical TOC Entry